International Journal of Biological Macromolecules 321 (2025) 146552

Contents lists available at ScienceDirect

International Journal of Biological Macromolecules

journal homepage: www.elsevier.com/locate/ijbiomac

Characterization and release modelling in ELR-based nanocomposite hydrogel loaded with polylactic acid for the implementation of a biomedical device

Julio Fernández-Fernández [a,b], Luis Quintanilla-Sierra [a,b], Oscar Castaño [c,d,f], Tosca Roncada [d], J. Carlos Rodríguez-Cabello [a,b], Matilde Alonso [a,b], Elisabeth Engel [e,d,f], Mercedes Santos [a,b,*]

[a] G.I.R. Bioforge, University of Valladolid, CIBER-BBN, Paseo de Belén 19, Valladolid, Spain
[b] Laboratory for Disruptive Interdisciplinary Science (LaDIS), University of Valladolid, 47011 Valladolid, Spain
[c] Electronics and Biomedical Engineering, University of Barcelona (UB), Marti i Franques 1, Barcelona, Spain
[d] Institute for Bioengineering of Catalonia, Barcelona Institute of Technology (BIST), Barcelona, Spain
[e] IMEM-BRT group, Materials Science and Engineering, Polytechnical University of Catalonia (UPC), Barcelona, Spain
[f] CIBER en Bioingeniería, Biomateriales y Nanomedicina, CIBER-BBN, Madrid, Spain

ARTICLE INFO

Keywords:
Hydrogel
Nanocomposite
Elastin-like recombinamers
Polylactic acid
Early and sustained release

ABSTRACT

Cardiac tissues are difficult to regenerate due to the low proliferative capacity of cardiomyocytes. A new therapeutic strategy for cardiac regenerative medicine could include a device capable of ensuring cell grafting, stimulating cardiac tissue regeneration, and serving as an appropriate scaffold for the controlled and sustained release of lactate over time as an inducer of cardiomyocyte proliferation. An effective source of lactate could consist of the lactic acid polymer (PLA) itself, which generates free lactic acid during its degradation. In this work, we have developed a nanocomposite hydrogel for lactate release based on a biocompatible and biodegradable matrix formed by elastin-like recombinamers cross-linked via click chemistry. Polylactic acid particles were encapsulated in the matrix after these particles had been partially degraded to lactic acid through oxygen plasma treatment. In the first 48 h, an early and modulated release of free lactic acid from plasma-treated PLA degradation is observed, and over longer periods, a sustained release of lactic acid produced by the hydrolytic degradation of PLA under physiological conditions occurs. Lactate is available from the very beginning ("early release"), addressing the drawback of the slow degradation (by hydrolysis) of polylactic acid. Therefore, a biomedical device has been designed and implemented, formed by an ELR polymeric matrix as an analogue of cardiac tissue, acting as a device for early, controlled, and sustained lactate release, with dosing at concentrations similar to those previously studied as suitable for promoting cardiomyocyte proliferation, showing promise for its use in the regeneration of infarcted cardiac tissue.

1. Introduction

Cardiovascular diseases (CVDs) are among the most significant human health problems and the leading cause of death, accounting for approximately 32 % of global deaths and resulting in the loss of around 18 million lives each year [1,2]. Cardiac lesions, such as those occurring after a myocardial infarction, lead to cardiomyocyte death and subsequent fibrotic tissue deposition and scar formation, which reduces cardiac contractility and causes heart failure [3].

Unlike fetal cardiomyocytes, adult cardiomyocytes have lost their proliferative capacity and are unable to regenerate. However, it is known that fetal cardiomyocytes, present in a lactate-rich environment such as the placenta, can take up lactate as an energy source [4]. Engel et al. have demonstrated that lactate induces changes in gene expression, leading to dedifferentiation and proliferation of mammalian cardiomyocytes, potentially mimicking a fetal-like environment conducive to regeneration [5]. Lactate activates a specific genetic program driven by the expression of BMP10, LIN28 and TCIM, among others, while also downregulating DGKK, GRIK1, and various ion channels related to adult cardiomyocytes. The upregulation of BMP10 induces cardiomyocyte proliferation and prevents the maturation of cardiac cells generating a pro-regenerative environment within the heart tissue [6,7]. Thus,

* Corresponding author at: G.I.R. Bioforge, University of Valladolid, CIBER-BBN, Paseo de Belén 19, Valladolid, Spain.
E-mail address: msantos@uva.es (M. Santos).

https://doi.org/10.1016/j.ijbiomac.2025.146552
Received 30 December 2024; Received in revised form 31 July 2025; Accepted 2 August 2025
Available online 5 August 2025

lactate supplementation has been shown to induce reprogramming of cardiac tissue to a fetal-like phase, in which cell proliferation is crucial for the development and growth of tissue and organ structures and functions.

On the other hand, lactate is a degradation product of biomaterials such as polylactic acid and its analogues and derivatives. Therefore, these biomaterials can be used as an effective source of lactate for cases of myocardial infarction or cardiac injury, thus mimicking the production of lactate by the placenta during fetal development. An approach for the regeneration of infarcted cardiac tissue could involve the development of a biomedical device for the controlled and sustained release of lactate over time. However, it is well known that regeneration of infarcted tissue must be induced within a short period of time after myocardial infarction, as scar tissue, and therefore non-functional tissue, forms within a few days [8]. In this regard, an ideal lactate release system would be one that releases it into the environment immediately upon insertion into the organism. However, polylactic acid (PLA) does not generate lactate immediately, and its release in the injury area would only occur after PLA degradation, which takes a relatively long period [9].

Hydrogels are three-dimensional (3D) structures formed by crosslinking between polymer chains. Their properties and characteristics, which enable them to emulate the extracellular matrix, make them excellent candidates for biomedical applications. Moreover, hydrogels can be loaded with different types of materials and drugs, giving rise to what is known as a composite hydrogel [10]. A composite hydrogel consists of the combination of two or more constituents at a macroscopic scale, while preserving their individual properties. Nevertheless, some specific characteristics of the composite may differ from those of the individual components. The porous 3D hydrogel network –named the matrix- can be loaded with fibers, particles (powder), sub-micron scale particles or structures ("nanoparticles"), flakes and so on [11–13], which allows the composite to be used for a variety of functions and applications [14].

Hydrogels can be loaded with several types of organic or inorganic nanoparticles, giving rise to what is known as a "nanocomposite hydrogel" [15]. Nanoparticles in the hydrogel may play two different roles: first, as a nanofiller, where their inclusion in the hydrogel matrix results in the enhancement of the properties of the unloaded matrix; and second, as a crosslinker, interacting with the matrix molecules, and then, participating in the overall composite crosslinking, along with the physical and/or chemical crosslinking of the matrix itself, which leads to changes in the strength and stiffness of the hydrogel [11]. For instance, recent reviews have shed light on the promising potential of composite hydrogels for bone defect treatments [16] and injectable hydrogel-based nanocomposites for CVD therapies [17]. These reviews emphasize the significant advancements, demonstrating that these innovative materials hold substantial promise for medical treatments [10].

Elastin-like recombinamers, ELRs, are genetically engineered polypeptides inspired by the peptides found in tropoelastin, the monomeric unit of native elastin. Elastin is the extracellular protein found in higher animals [18] that imparts elasticity and resilience to different organs and tissues, such as lungs, skin or blood vessels [19]. The amino acid sequence of ELRs, as they are produced recombinantly, can be fine-tuned to encode the required bioactive domains for biomedical and nanotechnological applications [20,21].

ELRs are intrinsically disordered protein polymers (IDPPs) with lower critical solution temperature (LCST) behaviour and exhibiting liquid-liquid phase separation (LLPS) with temperature [19,22]. Furthermore, ELRs are capable of creating polymeric networks with tissue-like nature. These scaffolds have been used for tissue-specific regeneration by controlling both the mechanical properties of the matrix as well as its biological properties. In fact, protein-engineered scaffolds with exceptional properties for the regeneration of various tissues, such as cartilage [23], skin [24], bone [25], cardiovascular [26] and, (especially relevant to this work) muscle tissue [27], have been fabricated. They have demonstrated the ability to spatiotemporally control the colonization of the scaffold by introducing protease-sensitive sequences of different kinetically controlled rates, thereby facilitating the regeneration of complex processes like angiogenesis and neurogenesis [28–30].

We highlight the possibility of preparing these scaffolds through click methodology, as ELRs can be decorated with crosslinkable functional groups such as azido or cyclooctynyl [31,32]. The strain-promoted [3 + 2] azide-alkyne cycloaddition (SPAAC) is a "click reaction" known to be highly efficient, atom-economical, fast, cytocompatible, and catalyst-free orthogonal approach suitable for physiological environments in living organisms [33,34].

In this work, we aim to design and implement a device for early and sustained release of lactate, with potential use in cardiac tissue regeneration. For this purpose, we will use a composite material whose three-dimensional matrix is formed by a chemical hydrogel based on the crosslinking of elastin-like recombinamers (ELRs) via click chemistry. This hydrogel will be composed of two ELRs, each endowed with the bioactive domains necessary for cell adhesion and degradation domains that facilitate complete tissue regeneration.

The embedded phase will consist of polylactic acid (PLA) particles, partially degraded through a plasma treatment, allowing for early release from the very beginning of the release process. Moreover, since the physiological degradation of PLA begins with a certain delay, lactic acid will be released continuously and sustainably over a long period. Finally, modelling the release kinetic according to various mathematical models will help to identify the dominant mechanism in each time frame.

2. Materials and methods

2.1. Design, synthesis and characterization of ELRs

The two ELRs used in this work, namely RGD-ELR and GTAR-ELR have been previously described [28,35]. Both ELRs are based on the repetition of the $((VPGIG)_2VPGKG(VPGIG)_2)$ elastin-like block. Both of them contain VPGKG pentapeptide located uniformly along the chain which will enable further chemical modification through the amine group of the lysines.

GTAR-ELR includes fast (GTAR) uPA-sensitive proteolytic sequences, while RGD-ELR contains the Arginylglycylaspartic acid domains that promote cell adhesion. The amino acid sequences are:

RGD:

$MGSSH_6SSGLVPRGSH\text{-}MESLLP\text{-}\{[(VPGIG)_2(VPGKG)(VPGIG)_2]_2\text{-}AVTGRGD\ SPASS\text{-}[(VPGIG)_2(VPGKG)(VPGIG)_2]_2]\}_6\text{-}V$

GTAR:

$MESLLP\text{-}\{[(VPGIG)_2(VPGKG)(VPGIG)_2]_2\text{-}YAVTGGTARSASPASSA\text{-}[(VPGIG)_2\ (VPGKG)(VPGIG)_2]_2]\}_4\text{-}V$

The ELRs were biosynthesized in a 15-L bioreactor and later purified by several cycles of temperature-dependent reversible precipitations, by centrifugation above and below their transition temperature (Tt) [36]. Subsequently, the ELRs were dialyzed against purified water and lyophilized. The purity and chemical characterization of the ELRs were verified by nuclear magnetic resonance (NMR) and matrix-assisted laser desorption/ionization time-of-flight (MALDI-ToF).

2.2. Chemical modification of the ELRs

Both ELRs were chemically modified by transformation of the ε-amine group from lysines to bear azide and cyclooctine reactive groups, respectively, as previously reported [31,37]. The modified biopolymers GTAR-cyclooctine was renamed GTAR-CC and the RGD-

azide was renamed RGD—N_3. The purity and chemical characterization of both ELRs were determined by nuclear magnetic resonance (NMR) and matrix-assisted laser desorption/ionization time-of-flight (MALDI-ToF) [36]. NMR and MALDI-ToF were performed at the Laboratory of Instrumental Techniques (LTI) of the Research Facilities of the University of Valladolid.

Both MALDI-ToF and ^{1}H NMR (in DMSO-d_6) were used to evaluate the degree of lysine chemical modification. In the case of NMR, the quantification of modified lysines in each ELR is achieved by integrating the signal of the amide proton, at 7.2 ppm, into which the amine group of the lysine has been converted after its modification. The number of actually modified lysines is determined based on this integral value (9 modified lysines of the total 16 lysines for GTAR-CC and 14 modified lysines of the total 24 lysines for RGD—N_3; Fig. S2A and S2B in Supplementary Information). Likewise, the modification of the lysines is corroborated through the molecular weight obtained for the modified polymer, considering the weight increase resulting from the modification of each lysine (113 g per modified lysine with an azide residue and 176 g per modified lysine with a cyclooctyne residue; Fig. S2C and S2D in Supplementary Information).

2.3. PLA treatment with plasma

2.3.1. PLA degradation treatment

Poly (L-lactic acid) (PLA) (Mw = 5000, PDI $\leq$ 1.2) was supplied by Merck Group. PLA powder was subjected to plasma treatment to achieve initial degradation of the polymer by breaking its ester bonds prior to being embedded in the hydrogel (gas flow mixer, PlasmaFlo, PDC-FMG-2, and Harrick Plasma cleaner, PDC-002-HP). The powder of PLA was deposited on Petri dishes in an amount of approximately 100 mg. Samples were placed into a reactor chamber and coupled plasma (argon and oxygen, at 20 mTorr and flow of 20 mL/min) treatments were carried out at high radiofrequency discharge (29.6 W) for 60 s with argon plasma, initially, and then with 15, 40 or 60 min of oxygen plasma, depending on the experiment.

2.3.2. PLA degradation control by FTIR and NMR

PLA degradation was monitored by infrared spectroscopy (FTIR-ATR) and ^{1}H NMR spectroscopy where we can monitor the appearance of the lactic acid produced after plasma treatment, as well as of the oligomers produced after random cleavage of the PLA chains.

The proportions of lactic acid produced concerning the PLA present in the samples were determined by nuclear magnetic resonance (NMR) using samples prepared in DMSO-d_6 at 5 mg/mL. Spectra were recorded using a 400 MHz Agilent spectrometer (Laboratory of Instrumental Techniques, University of Valladolid) with a 4 s relaxation delay between transients, 45° pulse width, 512 transients per sample and a spectral width of 6410 Hz. Proportions were determined by comparing the integrals of the signal for the methyl group from lactic acid with those of the methyl groups of polylactic acid. The spectra were analyzed using MestreNova v15 software.

Degradation monitoring is also carried out by measuring the FTIR spectra and by comparison of the spectra of untreated PLA with the spectra of PLA treated with oxygen plasma at specific times of 15, 40 and 60 min. Spectra were recorded using a Bruker TENSOR 27 acquiring 128 scans between 600 and 4000 cm^{-1} and a resolution of 4 cm^{-1}.

2.3.3. Lactic acid quantification

Upon completion of oxygen plasma treatment, the treated PLA samples were analyzed in order to quantify the lactic acid (LA) produced upon their degradation and, thus, the amount of LA embedded as free monomer in the hydrogels loaded with PLA.

The LA quantification is based on the measurement of the absorbance of samples treated with the NZYTech L-lactic acid determination kit and carried out with the SpectraMax iD5 spectrophotometer at a wavelength of 340 nm. The kit used is based on a stereospecific enzymatic method for the determination of L-(+) lactic acid (L-(+) lactate) using the reaction of lactic acid with NAD^+ (Nicotinamide Adenine Dinucleotide) in the presence of the enzyme LDH (L-Lactate dehydrogenase), measuring the absorbance of the NADH generated when lactate is oxidized to pyruvate.

Previously, a calibration curve was made from ten standard solutions, from 0 to 150 μg/mL, obtained by dilution from the commercial solution of concentration 150 μg/mL supplied in the kit. The absorbance data of the standard solutions, measured at 340 nm, were adjusted by a linear regression method to obtain the calibration curve (see Fig. S1 in Supplementary Information). The correlation equation obtained was:

$$\text{Concentration } [\mu g/mL] = 192.31 \bullet \text{Absorbance} + 0.54 \quad (1)$$

Likewise, the concentration of lactic acid produced in the plasma-treated samples is determined using the calibration curve obtained previously from the absorbance measured in the solutions prepared with 3 mg of treated PLA and 500 μL of PBS. The absorbance measurements are performed for the different plasma treatment times and with triplicates of the samples.

2.4. Preparation of lactic acid release systems: PLA encapsulation during hydrogel formation

Once the PLA has been treated as indicated in the previous Section 2.3.1, the active principles (PLA and lactic acid) are encapsulated into the hydrogels during their ("in-situ") formation. Gels were formed by catalyst-free click reaction for the orthogonal crosslinking between azide and cyclooctine groups from both modified ELRs chains [31]. This reaction exhibits high specificity for these functional groups, ensuring selective crosslinking within the ELR network. Solutions of GTAR-CC and RGD-N_3 were prepared in phosphate buffer saline (PBS, pH 7.2) at 75 mg/mL and kept at 4 °C overnight to ensure solubility. PLA-loaded gels were prepared in a separate tube were appropriate quantity of treated polylactic acid was introduced previously and, subsequently, combinations of cyclooctine- and azide-modified ELRs solutions were added at a 1:1 volume ratio (optimal crosslinking ratio [31]). Thus, 100 μL of 75 mg/mL HRGD-N_3 solution was added to the Eppendorf flask containing the PLA solid (3 mg), which is homogeneously resuspended with gentle agitation to avoid bubble formation. Immediately thereafter, 100 μL of 75 mg/mL GTAR-CC solution was added to that Eppendorf, gently shaking the mixture to achieve homogeneous distribution of the PLA. The mixture was then incubated at 37 °C for 15 min to obtain a consistent and homogeneous hydrogel with PLA properly dispersed. The incubation at this defined temperature plays a critical role in the hydrogel formation process, as it drives the ELRs to reach their inverse transition temperature, thereby promoting chain aggregation through hydrophobic interactions [38–40]. In addition, this process helps to make a homogeneous encapsulation of PLA within the hydrogel matrix. Before starting the dosing study, precautions were taken in order to eliminate any amount of PLA and LA on the hydrogel surface and not encapsulated –burst effect- and on the tips used for encapsulation.

2.5. Scanning electron microscopy micrographs and rheological measurements

Hydrogel morphology by SEM:

The structure and morphology of the nanocomposite hydrogel were evaluated by SEM. After the in vitro preparation described above, the samples were subjected to a physical fracturing process involving immersion in liquid nitrogen, followed by a second immersion in liquid nitrogen prior to freeze-drying. Once the samples had been lyophilized, they were metallized via a gold evaporator (SCD004 Model) with 30 mA and 40 s. Images of lyophilized hydrogels were obtained by SEM (HITACHI microscope, FlexSEM1000 model) with 10 kV voltage. Morphological details such as pore size were evaluated quantitatively

using the ImageJ software, averaging over 20 single pore sizes.

Rheological tests:

The first step for the preparation of nanocomposite ELRs-based hydrogels used in the rheological measurements consists of dissolving each ELR in PBS at 4 °C overnight (O/N). The hydrogel concentration studied was 75 mg/mL, with a molar ratio of 1:1. For each hydrogel, in an Eppendorf flask containing the untreated and plasma-treated PLA, 200 μL of GTAR-cyclooctine and 200 μL of RGD-azide were progressively added. Subsequently, the mixture of the three components was deposited in a specific 12 mm diameter mold to form hydrogels, which were incubated at 4 °C for 2 min. Subsequently, the samples were incubated for a period of 15 min at 37 °C. Three replicates were prepared and analyzed for untreated PLA and PLA with different treatment times.

A stress-controlled AR-2000ex rheometer (TA Instruments, New Castle, DE, USA) was used in order to carry out the rheological measurements. Cylindrical gel samples -submerged in water- were put between parallel plates of nonporous stainless steel (diameter of 12 mm), where a gap always higher than 1000 μm was used. No gel slippage occurs during the measurement due to the adequate choice of the normal force. Sample temperature was controlled and maintained at 37 °C using a Peltier device.

In order to measure the dynamic shear complex modulus, G*, as a function of strain, a dynamic strain sweep was accomplished at 1 Hz. The range of selected amplitudes was ranging between 0.01 and 15 %. Moreover, the linear region of viscoelasticity was delimited.

Significant viscoelastic moduli were determined: the elastic, G′, and loss, G″, moduli, and the complex modulus magnitude, $|G^*|$ $[|G^*|^2 = (G')^2 + (G'')^2$. Finally, the loss factor ($\tan\delta \equiv G''/G'$, where δ is the phase angle between the applied stimulus and the corresponding response) was also calculated. The measurements were made in triplicate.

Rheological characterization was completed by flow measurements where the dependence of the viscosity of the solutions with the shear rate was obtained. In these measurements samples were obtained following the description included in Section 2.4 with the exception of the last step (gelation step), namely, the incubation of the solution at 37 °C was excluded. Solutions were maintained at 5 °C before flow measurements, and then, deposited in the rheometer plate where the temperature was stabilized at 5 °C. Flow measurements were carried out at this temperature.

A circular parallel plate with a diameter of 40 mm was used to improve sensitivity. The volume of solution used in these measurements was 1250 μL. Each measurement includes two steps. First, a conditioning step was applied for 40 s at a constant shear rate of 0.5 s^{-1}. Immediately, and following a continuous ramp in a logarithmically ascending series of discrete steps, the shear rate was varied from 0.1 to 500 s^{-1}. In concrete, 10 measurements were acquired for each order of magnitude.

2.6. In vitro release studies

The in vitro release of lactic acid from hydrogels was carried out at 37 °C in a shaking incubator by adding 500 μL of phosphate buffer saline (PBS) to each sample of nanocomposite hydrogel.

From that point on, samples of the medium were taken at different time intervals, ranging from 1 min to 2 weeks. Each sample is collected, 60 μL, and replaced with equal volume of fresh PBS. The released sample was measured with the UV–Visible spectrophotometer. These experiments were carried out in triplicate.

2.7. Mathematical modelling of the drug release kinetics and mechanisms

Since the drug kinetic involves a complicated process, it is necessary to know the mechanisms of matter transport involved in drug release in order to quantitatively predict the release kinetics of the active ingredient.

Numerous models of the behaviour of material delivery devices were proposed in the literature, but we limit ourselves here to briefly mention the three fitting models we have used in our work [41–44]. These models were selected taking into account that they are the most used models for modelling the drug release from hydrogels. A short-time approximation is assumed for every model, namely, the model is able to properly describe only the first 60 % of the total drug release time [41,42].

i) Higuchi Model

Its well-known equation is the following:

$$\frac{Mt(t)}{M0} = k \bullet t^{0.5} \tag{2}$$

where (Mt/M0) is the fractional drug release at the release time, t, where M0 is the total drug load, and k is a kinetic constant that includes the drug diffusion coefficient. The only release mechanism considered in this model is Fickian diffusion [41,42].

ii) Korsmeyer-Peppas Model

The equation of this model is:

$$\frac{Mt(t)}{M0} = k \bullet t^{n} \tag{3}$$

where k is a kinetic constant incorporating structural and geometric system characteristics; and where n is the release or diffusional exponent that is related to the drug transport mechanism, and it has been estimated for cylindrical or spherical geometries when the release mechanism is diffusion, and even when other mechanisms may also be involved in drug release (see Table TS1 in Supplementary Information) [44].

iii) Peppas-Sahlin Model

The biexponential Peppas–Sahlin equation was also used to determine the contribution of both the Fick diffusion process and the relaxation/swelling of the polymer chains irrespective of the geometry of the release system [43].

In this case, its equation is:

$$\frac{Mt(t)}{M0} = kd \bullet t^{n} + kr \bullet t^{2n} \tag{4}$$

where n takes different values for different geometries and release mechanisms, kd and kr correspond to the Fickian diffusion constant and the polymer chain relaxation constant, respectively.

2.8. Cytotoxicity assay

The cytocompatibility of these materials was examined to confirm their potential use in cardiac tissue regeneration. Cell viability levels were determined using HL-1 Cardiac Muscle Cells, which were deposited on the hydrogels and composites, as well as on standard cell culture plate. Once the gels were deposited on the bottom of the wells (500 μL of ELR-based click unloaded hydrogels and composites containing 15 mg of treated or untreated PLA), cells at a concentration of 1×10^5 cells/mL (1 mL of medium) were deposited on them. They were cultured in 87 % Claycomb media, 10 % fetal bovine serum, 1 % penicillin/streptomycin, 1 % norepinephrine and 1 % L -glutamine. After 24 h, the medium was removed from the well and 10 % Alamar Blue was added, leaving the samples to incubate for 4 h at 37 °C. Cell viability was assessed by fluorescence and its concentration was determined by absorbance at 570 mm, which was measured using a microplate reader (Biochrom, U. K.). Viability in each well was calculated and normalized with respect to

the control (standard cell culture plate) as a relative percentage. The same procedure was followed at an additional 48 h of culture, obtaining cell viability measurements at 3 days.

2.9. Statistical analysis

Experimental data were obtained from triplicate measurements and reported as mean ± standard deviation (SD). These data were fitted by linear and nonlinear least-squares regression using Matlab (R2023a version). In the case of drug release experimental data were fitted only for the first 60 % of the time release. The fitted model parameters are reported as values with 95 % confidence bounds. Statistical comparison between groups was performed using a One Way ANOVA ($\alpha = 0.001$) followed by the Tukey and Bonferroni post-hoc test between each group.

3. Experimental results

3.1. ELR characterization

The modified elastin-like recombinamers, RGD-N_3 and GTAR-CC, were obtained as previously described [28,29,40] and their characterization is provided in Supporting Information (Figs. S2 A-D), confirming their correct chemical conversion.

3.2. Monitoring and optimization of PLA plasma treatment

Polylactic acid is a biodegradable biopolymer that, under physiological conditions, undergoes hydrolytic degradation to lactic acid monomer and oligomers, although the process is not immediate and depends on the medium in which it is found. The device designed for the "in situ" release of lactic acid, is formed by a hydrogel of ELRs that embeds PLA particles. These PLA particles, prior to their encapsulation in the gel, will be treated with plasma at different times in order to encapsulate both a source of lactate such as PLA, as well as the free lactate that is able to be released immediately at the application site. These plasma treatments break ester-like bonds and thus generate both monomeric lactic acid and oligomers of this lactic acid to different proportions depending on the treatment periods. Therefore, it is necessary to monitor the PLA degradation process by plasma treatment by means of several techniques such as: infrared spectroscopy to analyse the appearance of the new functional groups present in the monomers and oligomers produced in the treatment; ^{1}H NMR spectroscopy to detect the proportion of oligomers and lactate present together with the PLA degraded at different treatment times; and, finally, the accurate quantification of the lactic acid amount produced after each treatment cycle by absorbance techniques.

Thus, the correlation of these techniques will provide the optimization of the treatment time necessary for an adequate early and sustained release over time.

3.2.1. IR spectroscopy characterization

The infrared spectra of the samples treated with plasma at different times are shown in Fig. 1. The FTIR figure shows the spectrum of untreated PLA as a control, which shows a very sharp signal at 1750 cm^{-1} characteristic of the aliphatic ester bond absorption band [45].

As can be seen in Fig. 1, the plasma-treated samples show two new absorption bands not present in the untreated sample. The first band is particularly broad and occurs at wavelengths above 3000 cm^{-1}. This band corresponds to the absorption of the hydroxyl groups formed in the cleavage of the ester group of PLA [46]. As the sample treatment times increase, for 15 and 40 min, this signal increases. However, the samples treated 1 h with plasma show lower intensity in this hydroxyl band (Fig. 1B).

The other new band appears at 1725 cm^{-1} as a shoulder of the ester group signal present in PLA at 1750 cm^{-1} and corresponds to the carboxylic group of lactic acid that is formed after plasma cleavage of the ester group (Fig. 1C) [47]. In this case, as the plasma treatment time increases, for 15 and 40 min, a higher intensity is observed in that shoulder, as a consequence of the increase in the number of carboxylic groups present in the treated samples and belonging to lactic acid and its oligomers formed in the process. Again, a decrease in the absorption band at 1725 cm^{-1} is observed for the sample treated for 60 min.

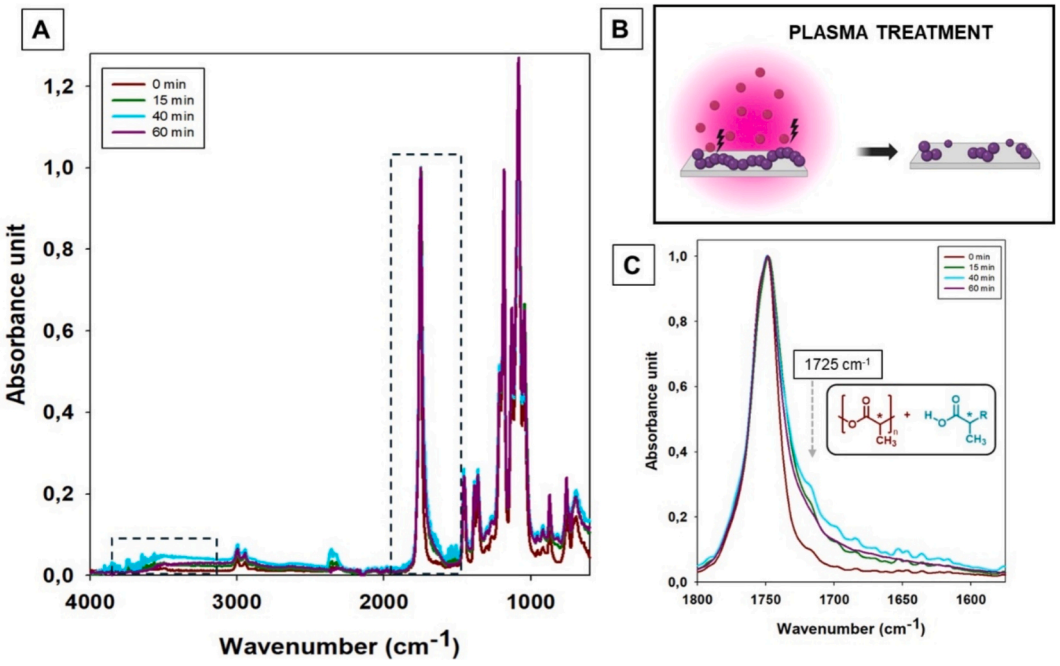

Fig. 1. A) FTIR Spectra of the PLA untreated (brown line) and of the PLA with different plasma treatment times (green, blue and violet for 15, 40 and 60 min, respectively). The dashed squares show the appearance of new signals. B) Representative drawing of the plasma treatment process. C) The zoom of the signals in the range between 1550 and 1800 cm^{-1} is shown, allowing a detailed observation of the peak corresponding to aliphatic ester bonds at 1750 cm^{-1}, together with a shoulder at about 1725 cm^{-1} assigned to carboxyl groups from lactic acid.

Therefore, the increase of the hydroxyl and carboxyl bands with treatment time for 15 and 40 min, indicating an increase in the number of lactate molecules and lactate oligomers, together with the lower absorption observed in these bands for longer treatments of 60 min, indicating a decrease in the proportion of lactate and its oligomers, allow 40 min as the optimal plasma treatment time for the samples to be considered. The decrease of lactic acid after 60 min of treatment time could be related to the cleaning and activating effect of the plasma that removes the lactate produced, just as it happens with organic matter in general [48].

3.2.2. NMR spectroscopy characterization

Along with the infrared spectra, we also carried out the study of the composition of the PLA samples treated with plasma at different times by NMR spectroscopy. The NMR spectra performed on the PLA samples treated with plasma at different times, as well as the untreated PLA itself, are shown in Fig. 2.

The NMR analysis of low molecular weight polylactic acids has been described in bibliography [49]. The authors describe the NMR spectra of lactic acid, its dimer, trimer and tetramer, as well as LA polymers, making an exhaustive study of the chemical shifts of the methyl and methine groups present in all these molecules. The results of that work have been used to determine the proportion of LA present in the plasma-treated PLA sample, from the integrals of the characteristic signals of both groups and whose different chemical shifts and integrals will allow us to determine the proportion of LA present in the treated PLA, as well as the different oligomers produced from PLA cleavage.

Fig. 2A shows the NMR spectra of the samples dissolved in DMSO-d_6 of PLA treated with plasma for 15, 40 and 60 min, as well as the untreated PLA as control. Fig. 2B shows the structure of the monomer, dimer, trimer, tetramer and polymer of lactic acid, as well as the chemical shift of its methyl and methine groups.

According to bibliographic reference 34, the signals corresponding to the methyl and methine groups at 1.23 and 4.03 ppm, respectively, have been assigned as belonging to lactic acid. Likewise, the signal at 1.46 and 5.19 ppm can be assigned as corresponding to the methyl and methine groups, respectively, present in the PLA chain. In the sample treated with plasma for 15 min, the appearance of the signal of the lactate

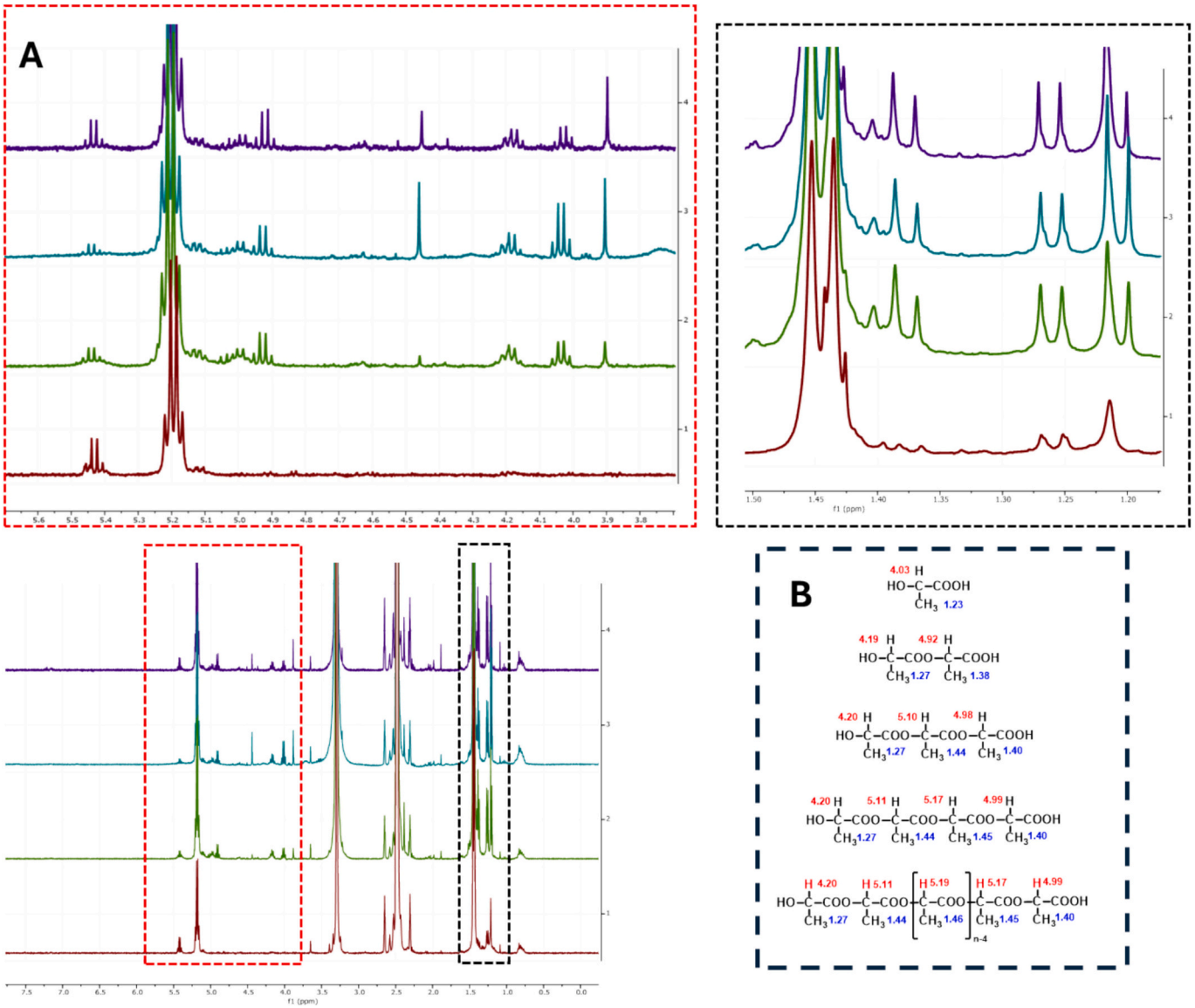

Fig. 2. A) NMR spectra of the PLA untreated (brown line) and the PLA with different plasma treatment times (green, blue and violet, for 15, 40 and 60 min, respectively) and two zooms of the signals in the range between 1.1 and 1.6 ppm (black dashed line square) and 3.7–5.7 ppm (red dashed line square); B) Chemical shifts of the protons of the methine and methyl groups for ^{1}H NMR spectra in DMSO-d_6 extracted from reference 34.

protons can be observed at 1.23 and 4.03 ppm, together with those of other lactate oligomers whose methyl group appears at 1.27 ppm and the methine groups as multiplet around 4.2 and between 4.9 and 5.2 ppm. At 40 min plasma treatment it is observed that the signal of the lactate methyl protons increases with respect to that of the oligomeric methyls, which is deduced from the higher integral of the methyl groups at 1.23 ppm versus those appearing at 1.27 ppm. From the value of the integrals of the signals of the methyl groups in the NMR spectra, the ratio between: lactic acid:oligomers: PLA is deduced. Thus, it is observed in Fig. S3 in Supplementary Information that the signals of this methyl at 15 min are in the ratio 4.3:4.3:39.0, while at 40 min said ratio is 5.3:3.2:36.8, showing an increase, from 4.3 to 5.3, for the signal at 1.23 ppm of lactate and a decrease, from 4.3 to 3.2, for the integral of oligomeric methyl group at 1.27 ppm (Fig. 2 and fig. S3). From the control of these two treatment times, we deduce that the breakdown of the PLA polymeric chain occurs to a greater extent as the plasma exposure time increases and, therefore, the proportion of lactic acid generated is higher.

After 60 min of treatment, however, the lactate methyl signal at 1.23 ppm decreases (see zoom of Fig. 2A) and the spectrum shows a much more "complex" appearance showing the presence of oligomer mixtures along with other products of possible polymer degradation. In view of the NMR spectra, and in agreement with the infrared spectroscopy results, when the plasma treatment time increases up to 60 min, there is a decrease in the proportion of lactate and oligomers in the sample which, as previously indicated, may be due to the organic matter scavenging role of the plasma itself [48]. For this reason, we selected 40 min as the upper bound in the plasma treatment time for PLA.

Once determined, by both FTIR and NMR, the increase in LA production with the PLA treatment time -with the upper bound plasma treatment time of 40 min, we calculated the amount of lactic acid produced from the PLA degradation by means of absorbance measurements of the samples at 0, 15, 40 and 60 min.

3.2.3. UV–visible spectroscopy quantification of the amount of lactic acid

The quantification of lactic acid present in the samples of PLA treated with oxygen plasma was performed with NZYtech kit as described in Section 2.3.3 from the absorbance data. Thus, the calibration curve obtained as described in this subsection will be applied to the experimental absorbance data to calculate the lactic acid concentration of each sample.

To quantify the amount of lactic acid initially encapsulated in the release device and formed by the degradation of the polymer due to the O_2 plasma treatment, samples of each PLA (3 mg) were analyzed after being treated with plasma at different time points: 0, 15, 40 and 60 min of plasma treatment as before mentioned.

No lactic acid amount was detected for the PLA untreated with plasma, and therefore, no free monomer at all was initially encapsulated. For the PLA treated for 15 min and 40 min, 47.5 μg and 63.1 μg of free LA are initially encapsulated in the hydrogel, which corresponds to 1.6 % and 2.1 %, respectively, of the total PLA. However, for the PLA sample treated for 60 min, the free lactic acid quantified was only 51.8 μg, 1.7 % of the total PLA.

3.3. Morphology and mechanical properties of the unloaded and loaded hydrogel

3.3.1. Morphology of the gels by SEM

The preparation of click hydrogels is carried out according to the methodology described in Section 2.4. Hydrogels without PLA (unloaded), with untreated PLA and with treated PLA were prepared and the videos of the preparation of the hydrogels can be found in the additional documentation of the article. As shown in the hydrogel formation videos, the homogeneous suspension of the treated PLA is favored by the higher polarity of the polymers present, which have a higher proportion of carboxyl and hydroxyl groups relative to untreated PLA, as demonstrated by analysis of their infrared and NMR spectra.

The morphology and structure of the ELR-based hydrogel and composites were described by scanning electron microscopy from the study of the samples prepared according to the methodology described in Section 2.5. Fig. 3 shows the images taken for both the unloaded hydrogel and the composites prepared with untreated PLA and PLA treated with plasma for 15 and 40 min.

For the unloaded hydrogel, regular and ordered porosity with high interconnectivity was observed. Quantitative analysis of SEM micrographs provided an average pore size of 9.0 ± 2.5 μm. These results agree with the morphology of these hydrogels reported by Flora et al. [28].

When untreated PLA is included in the matrix, small spherical structured particles are observed, while they are not present in the unloaded matrix (Fig. 3A: vi and x vs. v and ix). The zoom of the pores network (second and third row with scale bar of 20 and 10 μm, respectively) shows that the particles are on the wall pore, which is flat and smooth without aggregations. Two main size particle populations have been found with diameters 80 ± 14 nm, and 380 ± 90 nm. For this composite, an average pore size of 16.6 ± 1.9 μm was estimated.

For the 15 min PLA treated sample, the nanocomposite hydrogel shows a highly porous network, with well-defined pores, but the wall of which is rough and disturbed. Finally, for the 40 min PLA treated sample, a significant amount of the pores have lost their integrity and have appeared as "broken" or open pores with aggregations and roughness on the wall pore. For both treated samples, an average pore size of 13.80 ± 2.70 μm, and 63 ± 20 μm was found, respectively. As can be seen in Fig. 3B, the average pore size in the untreated or 15 min-treated composite increases with respect to the unloaded hydrogel, but it is the 40 min-treated composite where the pore size shows a noticeable rise. The differences were significant when comparing the pore sizes in the sample with untreated PLA and PLA treated for 15 min with the samples containing PLA treated for 40 min; and, clearly, with the sample that does not contain PLA. Finally, there are no significant differences between the sample loaded with untreated PLA and the one loaded with PLA treated for 15 min. As for the standard deviation, similar values are found for all samples, except for the one treated for 40 min, where a greater distribution of pore sizes is observed, indicating a higher degree of inhomogeneity.

Greater interaction between the polylactic particles and the ELR matrix is corroborated by the fact that in the case of the untreated polylactic particles when we obtain the SEM image of the fractured surface, clearly differentiated particles from the matrix are observed, more or less spherical, exposed, and embedded in the hydrogel matrix. However, when the polylactic samples have been treated, rounded and smoother shapes are observed, with an appearance different from the previous case and similar to the ELR matrix. From this, it can be deduced that due to the establishment of strong interaction forces, such as hydrogen bonds and charge affinity, between the treated polylactic particles and the crosslinked ELR matrix, the polylactic particles are completely covered by the ELR. This strong interaction is not present in the untreated polylactic samples.

Another effect that can also be observed in the SEM images as a consequence of the favored interaction between the two phases of the nanocomposite is that the pore size in the samples is different, despite the fact that the concentrations and volumes of the ELR solutions used were exactly the same in all the samples. More specifically, the samples exhibit a non-homogeneous distribution of ELR in the samples with treated polylactic particles. In these samples, there is a greater compaction of ELR polymer molecules around the treated polylactic particles due to the strong interaction present; this draws ELR molecules away from the rest of the sample, resulting in a structure with larger pore sizes of 63 ± 20 μm for 40 min treated samples.

3.3.2. Mechanical properties for the hydrogels: rheological measurements

The mechanical characterization of the hydrogels was carried out by

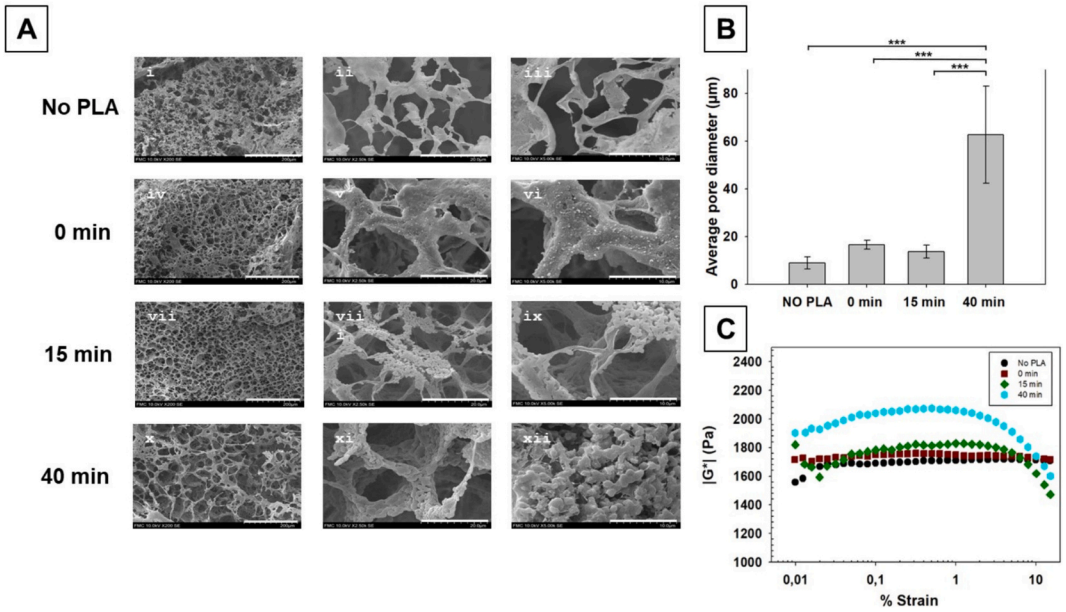

Fig. 3. A. SEM micrographs for the sample with an ELR concentration of 75 mg/mL in all cases; without PLA or with PLA, untreated or plasma treated for 15 min or 40 min (located at the rows), at three different magnifications (scale bar: first column (i; iv; vii; x), 200 μm; second column (ii; v; viii; xi), 20 μm; and, third column (iii; vi; ix; xii), 10 μm). B. Histograms showing the average pore size diameter and its corresponding standard deviation calculated from the SEM images using the ImageJ program. *** $p < 0.001$. C. Representative rheological curves of the dependence of the complex modulus magnitude on strain amplitude at a frequency of 1 Hz and at 37 °C for the same samples.

rheological measurements in oscillatory mode (specifically, a strain sweep was accomplished) at a temperature of 37 °C. The linear viscoelastic range is extended up to 6–7 % strain amplitude –namely, interval where the magnitude of the complex modulus is approximately independent of the strain amplitude- according to Fig. 3C. As can be seen, the complex modulus values remain in the same order of magnitude (around 1.5–2 kPa at a frequency of 1 Hz) for all the samples, but some changes are observed due to the PLA presence or the PLA time treatment.

This complex modulus value agrees with those moduli previously reported in the bibliography for the unloaded hydrogels for concentrations in the range 50–100 mg/mL [28], which was chosen since hydrogels exhibit similar mechanical properties to that of scaffolds used to regenerate soft tissues [50].

Similar values in the complex modulus are observed for unloaded PLA and for untreated loaded PLA hydrogels. In the case of plasma treated hydrogels it is found an increase in this modulus that is more evident for the 40 min treated PLA samples (Fig. 3C). The changes in the mechanical properties of the composite measured by rheology show the reinforcement of the polymeric network in the presence of stiffer PLA solute [51].

Detailed values of the elastic and loss moduli -corresponding to the complex modulus magnitude in rheological curves of Fig. 3C- have been included in the histograms of Fig. S4. A smooth and continuous increase of the elastic modulus is observed for the untreated and 15-min-treated composites with respect to the unloaded hydrogel, while the increase is somewhat higher for the 40-min-treated sample. As far as the loss modulus is concerned, the mere presence of PLA (without treatment) decreases this modulus, while plasma treatment changes this trend. Thus, while similar values are observed for the untreated and 15-min-treated samples, a remarkable increase is observed for the 40-min-treated sample.

The rise in the elastic modulus indicates an increase in cross-linking of the composite. Focusing our attention on the 15 and 40-minute-treated composites, the degraded PLA has generated oligomers and lactic acid itself that possess hydroxyl and carboxyl groups. The presence of these polar groups was corroborated by infrared spectroscopy (see Section 3.2.1) and the presence of lactic acid and different oligomers, together with PLA itself, was verified by NMR spectroscopy (see Section 3.2.2). The presence of these polar groups may give rise to intermolecular interactions -such as hydrogen bonds or dipole-dipole interactions- between the matrix elastin-like polymeric chains and the PLA derivatives, which operate as a so-called physical crosslinking, in addition to the chemical crosslinking of the ELR matrix itself. The moderate increase observed in the elastic modulus is compatible with the weaker strength of these physical interactions (see, for instance, [52]). Nevertheless, the higher the plasma treatment time, the higher the amount of polar groups available to interact, and the higher the elastic modulus; thus, this modulus increases by around 16 % for the 40-min-treated sample with respect to the untreated one (see Fig. S4).

As an overview of the morphology study by SEM and the rheological characterization of the nanocomposite hydrogel, we can infer that the samples treated for 15 and 40 min show a differentiated internal structure with globular structures of particles coated with ELR and a different mechanical behaviour compared to the unloaded hydrogel or the untreated PLA sample (0 min). However, the increase in pore size is not evident until a 40-minute PLA treatment is performed, which enhances the prevalence of hydrogen bonding and dipole-dipole interactions between the load and the ELR hydrogel.

In Fig. S4 (C) the evolution of the viscosity as a function of the shear rate has been drawn in a lin – log scale for the sample without PLA and the untreated and treated samples with PLA. As can be seen, none of the samples show a Newtonian regime in viscosity. Instead, and according to the shear rate dependence, two different regions -each of them showing a clearly different slope- are observed in each curve. The boundary between these regions is about a shear rate of 2–3 s^{-1}. A similar behaviour was found in another ELR previously reported in bibliography [53]. Thus, the increase of shear rate gives rise to a decrease in viscosity and, therefore, our samples can be considered in the category of shear-thinning hydrogels, which facilitates injectability.

The lowest viscosity is measured for the sample without PLA, whereas the incorporation of PLA increases the viscosity for the untreated and treated samples. For a shear rate higher than 20 s^{-1} the viscosity is similar for all the samples, and eventually, the curves tend to overlap.

In addition to the mechanical properties already presented above and the favourable results obtained in the viscosity test, an extrusion experiment using a Luer-Lok TM syringe equipped with a 20G needle has been performed to evaluate the injectability of the system. As shown in the attached video, the material can be injected with ease, comparable to that of a liquid component, in agreement with the quantitative viscosity data. After injection on a tempered plate at 37 °C, the liquid hydrogel gels almost instantaneously, forming a three-dimensionally stable structure. This same reproducibility is also observed when extruding the control system without PLA (see attached videos and images from Fig. S4D). These shear thinning results and rapid gelation make these systems ideal candidates for applications where injectability is key.

3.4. Release kinetics of LA treated with plasma

Following the methodology described in Section 2.4, Fig. 4 shows the evolution of the lactic acid released over time for the untreated, treated for 15 min, and treated for 40 min composites. The total amount of load in all cases was 3.0 mg, which will be either all PLA or a combination of PLA and LA, depending on the case.

For the untreated composite, up to a time point of 48 h, no lactic acid released is detected. After 48 h, the LA release begins due to the hydrolysis of the PLA within the hydrogel and the amount of lactic acid released increases with time for the entire period tested. For times longer than 200 h, an approximately linear evolution on time is found whose slope is 360 ng/h (Fig. 4B).

For the composite with PLA treated for 15 min, the initial mass amount of lactic acid-free encapsulated in the hydrogel is 47.5 ± 2.3 μg. In other words, of the 3.0 mg of total PLA encapsulated in the hydrogel, 47.5 μg were lactic acid resulting from the O_2 plasma treatment for 15 min. For this sample, as shown in Fig. 4A, lactic acid release begins at 15 min. By 48 h, the amount released approximates the initial encapsulated free lactic acid amount. Thus, the lactic acid produced by the 15-min treatment plasma is released within the first 48 h of the assay. After 48 h, the lactic acid produced from PLA hydrolysis also begins to be released as observed for the device with the untreated PLA sample. In these 15-min-treated samples, the LA released amount reaches a maximum of 75.0 ± 0.9 μg for time points around 200 h (around 60 % of the total release time considered in this work) in this cumulative release method. For times longer than 200 h the measured amount of free LA decreases (Fig. 4B).

Finally, for the composite treated for 40 min, its initial encapsulated mass of free lactic acid is 63.1 ± 1.9 μg, which is the maximum amount that can be released in the first 48 h before PLA hydrolysis occurs. In this case, the release of lactic acid began at the start of the assay (see Fig. 4A). The lactic acid produced by the 40-min plasma treatment is dosed in the first 48 h of the assay, and as can be seen in the graph, approximately 65.0 μg of LA were released in this time. After 48 h, the lactic acid produced by hydrolysis is also released, resulting in higher values. The maximum release amount reached 92.5 ± 4.4 μg, and although the process is cumulative, it begins to decrease for times longer than 150 h, similar to the sample treated for 15 min (Fig. 4B).

The decrease in the lactate concentration found for the two plasma-treated samples may be explained as follows. Dusselier and co-workers [54] found that a 90 wt% lactic acid solution at equilibrium contains only 65.9 wt% free LA, while 25.0 wt% is in the form of lactic dimer. Thus, due to the instability of L-lactic acid against its dimers and oligomers, LA tends to esterification towards lactoyl units (linear dimer of lactic acid), and even to lactic oligomers when aqueous solutions are more concentrated, in a reversible esterification process [54]. In our treated samples, Fig. 4 shows that the peak cumulative amount of lactic acid release for the treated samples is about 3–4 times higher than that of the untreated one, generating the instability of lactic acid, that is not

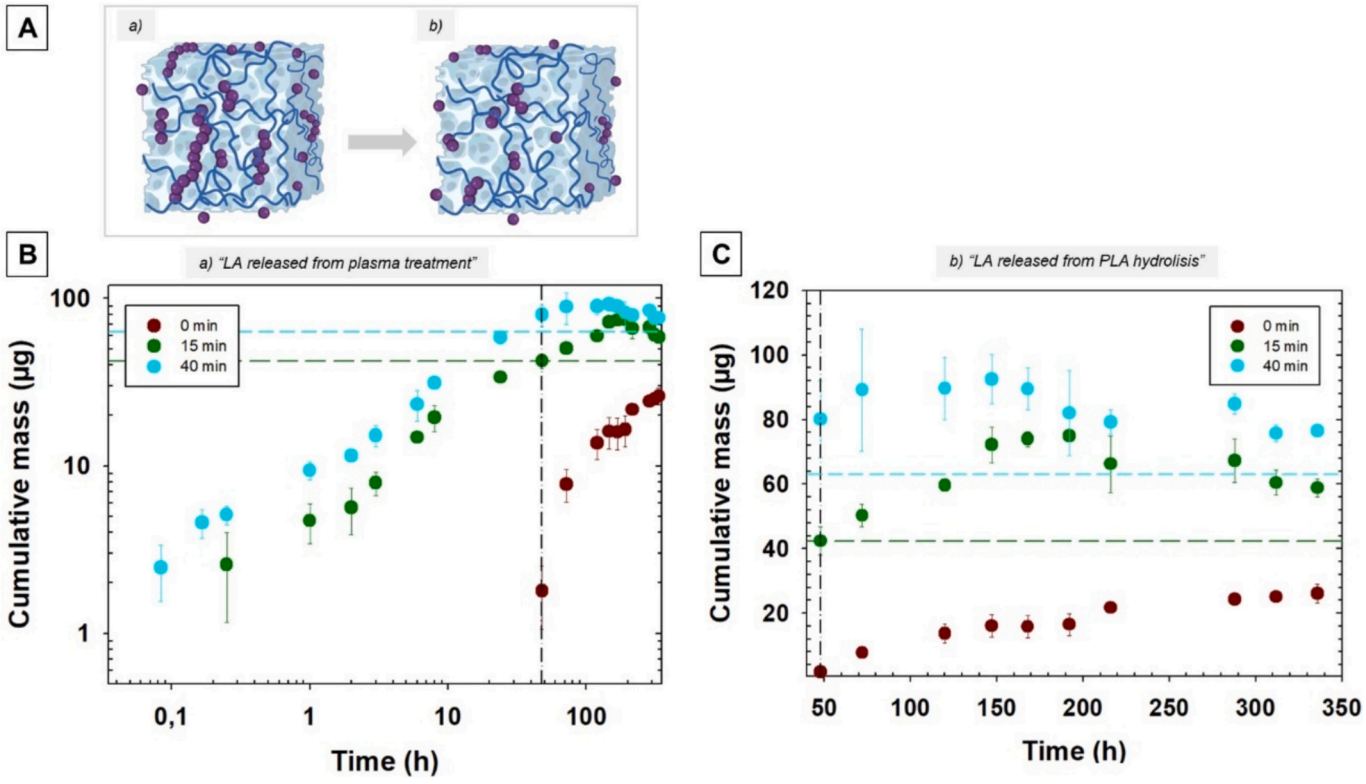

Fig. 4. Cumulative mass released of lactic acid as a function of time for PLA O_2 plasma treatment of 0 min (without treatment, brown dots), 15 min (green dots), and 40 min (blue dots). A. Cartoon of the composite a) in the first time frame ($t < 48$ h) and b) at $t > 48$ h. B. $\log_{10}$ - $\log_{10}$ scale has been used for release curve. C. A zoom of the release curve for times between 48 h and 350 h has been plotted in a lin – lin scale. The vertical black dashed line indicates the time point at 48 h. The free lactic acid encapsulated, produced in each PLA plasma treatment, is indicated by horizontal dashed lines of the respective colours green (15 min) and blue (40 min).

observed for the untreated sample.

In consequence, at longer times we assume that two processes are simultaneously operating in the treated samples: first, similarly to the sustained release observed for the device with untreated PLA, the lactic acid from PLA hydrolysis continues to be produced; and second, the transformation of lactic acid by esterification to the dimer or oligomers.

As the amount of dimer and oligomers of lactic acid cannot be measured with the method of analysis used in our work, the lactic acid net decrease measured in our cumulative release may be attributed to the esterification of the lactic acid present in the medium. This net decrease begins around 150 h for the 40 min treated sample, a shorter time than that of the sample treated for 15 min, due to the higher concentration of lactic acid in the medium in this cumulative release.

In summary, the time it takes to release all the free lactic acid obtained from the PLA treated with O_2 plasma for both the 15 min and the 40 min treated one is around 48 h. The onset of lactic acid release in the composite treated for a longer time with plasma occurs earlier, since the longer the plasma treatment time, the greater the degradation of the polymer and, consequently, the greater the amount of free lactic acid monomer able to be released. For the period between 48 and 150 h, we observed a continuous release of lactic acid in all three devices where the progressive hydrolytic degradation of PLA plays a fundamental role (Fig. 4A).

In the time interval of 0.5–150 h an approximately linear evolution with two different slopes is found in a $\log_{10}$ - $\log_{10}$ scale, indicating a mathematical relationship where the released mass is proportional to a power of time, in agreement with the modelling of the drug release kinetic introduced in Section 2.7 ($M_t(t)/M0$ is proportional to t^n). Thus, in this scale the slope corresponds to the release exponent, n (Fig. 4B).

As can be seen in Fig. 4B, a comparable slope is found for the two plasma-treated samples, in the range 0.5–48 h, irrespective of treatment time. An analogous behaviour is observed in the 48–150 h time frame (Fig. 4A). Therefore, a similar release exponent is suggested, and then, the same release mechanism in each time range.

3.5. Cytocompatibility

Cell viability was evaluated on days 1 and 3, and the results generally showed good viability across the different samples analyzed (Fig. 5). On day 1, no significant differences were found between the culture plate control (2D) and the other conditions. On day 3, the conditions—culture plate control (2D), ELR hydrogel (NO PLA), and ELR composite containing treated PLA (PLA TREATED)—again showed no significant differences among them. However, all three exhibited statistically significant differences compared to the composite sample with untreated PLA (PLA NOT TREATED) ($p < 0.001$), which showed considerably lower viability. These results suggest that both the hydrogel without PLA and the hydrogel incorporating treated PLA support good cell viability, comparable to that of the standard 2D culture, confirming their cytocompatibility.

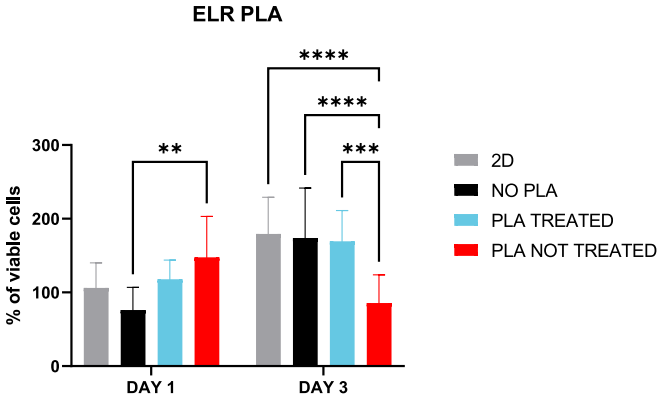

Fig. 5. Cell viability assessment of ELR-based hydrogels without and with PLA (treated and untreated) at days 1 and 3, using the Alamar Blue assay on HL-1 cardiomyocyte cells. Results are expressed as the percentage of viable cells relative to the 2D control at day 1. From left to right, bars represent cell viability for: culture plate control (2D), ELR hydrogel without PLA (NO PLA), ELR composite containing treated PLA (PLA TREATED), and ELR composite containing untreated PLA (PLA NOT TREATED). Each bar represents the mean ± standard error (SE) of twelve independent experiments. Statistical analysis was performed using one-way ANOVA (** $p \leq 0{,}01$; *** $p \leq 0.001$; **** $p \leq 0.0001$).

The good cytocompatibility of the ELR composite with treated PLA is particularly relevant, as this sample exhibits optimal release performance in this study and is expected to have a greater effect on cardiomyocyte activation.

4. Discussion and modelling of release mechanisms

According to the release assays, two different and independent evolution kinetics were observed in different time ranges. Therefore, two-time frames were considered to get a more accurate description of the process.

For samples submitted to O_2 plasma treatments, the first graph (Fig. 4A) gathers the dosage values up to 48 h, where "early release" is observed for both samples treated for 15 min and 40 min. PLA hydrolysis did not yet occur so the only amount of lactic acid that can be released was produced by the plasma treatment. The second graph (Fig. 4B) shows the remaining values, after 48 h and up to 200 h, where lactic acid is already the result of the hydrolytic degradation of the polymer chains. In these later curves, the time origin has been shifted in the graphical representation to start from 0 s.

For the pristine sample, only the time frame starting at the 48-h hydrolysis period has been considered, as the lactic acid concentration in earlier periods cannot be detected.

Experimental data were fitted to the three considered models whose corresponding parameters were numerically calculated by using a non-linear least-square regression method assuming a short time approximation (in our case the 60 % of the time considered corresponds to times not higher than 200 h) [41,42].

The experimental release data and the model providing the best fit can be found in Figs. S5 to S7 in Supplementary Information; its corresponding fitting parameters have been summarized in Table 1. These same experimental data and their fit to the discarded models have been assembled in Fig. S8 (see Supplementary Information); the value of these parameters is shown together in Table TS2 in Supplementary Information.

Table 1
This table summarizes the model and the corresponding parameters that provide the best fitting to the experimental release data.

Time (h)	Fitting model	n (with 95 % confidence bounds)	k (s^{-n}) (with 95 % confidence bounds)	R^2
PLA treated with O_2 plasma for 0 min (without treatment)				
$t \geq 48$	Higuchi	0.5	$7.310 \cdot 10^{-6}$ ($6.739 \cdot 10^{-6}$, $7.88 \cdot 10^{-6}$)	0.979
PLA treated with O_2 plasma for 15 min				
$t \leq 48$	Korsmeyer-Peppas	0.5772 (0.4342, 0.7201)	$8.7554 \cdot 10^{-4}$ ($7.701 \cdot 10^{-4}$, $9.800 \cdot 10^{-4}$)	0.955
PLA treated with O_2 plasma for 40 min				
$t \leq 48$	Korsmeyer-Peppas	0.6207 (0.5193, 0.7221)	$7.997 \cdot 10^{-4}$ ($7.438 \cdot 10^{-4}$, $8.557 \cdot 10^{-4}$)	0.978
$200 > t > 48$	Higuchi	0.5	$1.764 \cdot 10^{-5}$ ($1.696 \cdot 10^{-5}$, $1.831 \cdot 10^{-5}$)	0.998

- PLA without O_2 plasma treatment: untreated PLA

To model the release behaviour of the composite with untreated PLA, the total amount of polylactic acid encapsulated in the hydrogel was considered as the M0 value. Since 3.0 mg of PLA were encapsulated in the hydrogel, the value of M0 is 3000 μg.

The kinetic evolution of the release, Mt.(t)/M0, and the model that best fitted the experimental data -the Higuchi model- have been plotted in Fig. S5 (see Supplementary Information). A value of $k = 7.310 \bullet 10^{-6}$ $s^{-0.5}$ (correlation coefficient, $R^2 = 0.979$) was obtained. According to this model, the mechanism dominating the release of lactic acid formed by the hydrolytic degradation of PLA inside the gel is Fickian diffusion.

The fit to the Korsmeyer - Peppas model was discarded for giving inconsistent values of the kinetic constant, k, with an error greater than the value itself (see Fig. S8(a), and Table TS2 in Supplementary Information).

The fit to the Peppas-Sahlin model was also discarded for giving a negative value of kr (see Fig. S8(b), and Table TS2 in Supplementary Information). However, since this value is quite near zero, and taking into account the good correlation coefficient, this result can be interpreted as the Fickian diffusion contribution dominates over chain relaxation in agreement with the Higuchi model.

- PLA treated with O_2 plasma for 15 min

• Time up to 48 h

In this case, the initial mass of lactic acid-free produced from PLA via O_2 plasma treatment is considered as the value for M0 = 47.5 μg.

The Korsmeyer-Peppas model gives the best fit (Fig. S6 (a) in Supplementary Information) with parameters of $n = 0.58$ and $k = 8.755 \bullet 10^{-4}$ $s^{-0.58}$ ($R^2 = 0.955$). As the value of n is between $0.5 < n < 1$, the release process corresponds to an "Anomalous" transport whose release mechanism is based on both diffusion and swelling/relaxation of the polymeric chains.

In this time frame, Higuchi's model was discarded for having a low correlation coefficient in comparison to those of the other fits (see Fig. S8(c), and Table TS2 in Supplementary Information). The Peppas - Sahlin model was ruled out due to the negative value found in the kd parameter and the low n value (see Fig. S8(d), and Table TS2 in Supplementary Information) [43].

• Time ranging from 48 to 200 h

The best fitting model was the Higuchi model (Fig. S6 (b) in Supplementary Information), where the value of the parameter k was $2.107 \bullet 10^{-5}$ $s^{-0.5}$ ($R^2 = 0.981$). This result agrees with that obtained for the untreated PLA. Thus, a drug Fickian diffusion is again indicated in this timeframe where PLA hydrolysis is present (see Fig. 4B). The value of this kinetic constant is higher than the value obtained in the untreated PLA.

The fits to the Korsmeyer - Peppas and Peppas - Sahlin models were discarded since some parameters have an error higher than itself parameter (see Fig. S8 (e) and (f), respectively, and Table TS2 in Supplementary Information).

- PLA treated with O_2 plasma for 40 min

• Time up to 48 h

In this release, in the first part of the data, the value of M0 will be equal to 63.1 μg, which is the initial mass of lactic acid-free produced from PLA by the O_2 plasma treatment.

It is again the Korsmeyer-Peppas model that best fits (Fig. S7 (a) in Supplementary Information) the experimental data with parameters: $n = 0.62$, and $k = 8.0 \times 10^{-4}$ $s^{-0.62}$ ($R^2 = 0.978$). Similarly, to the PLA treated 15 min, in this case, the value of n is also between $0.5 < n < 1$, and the corresponding release process is an "Anomalous" transport.

In this case, the Higuchi model was also discarded for having a worse fit than the Korsmeyer - Peppas model (see Fig. S8 (g), and Table TS2 in Supplementary Information). Similarly to the 15 min treated sample, the fit to the Peppas - Sahlin model obtained a negative, very close to zero kr value, and with an error significantly higher than itself value in this parameter (Fig. S8 (h), and Table TS2 in Supplementary Information).

• Time from 48 to 200 h

The model that best fits the experimental data (Fig. S7 (b) in Supplementary Information) is the Higuchi model with a value of $k = 1.764 \bullet 10^{-5}$ $s^{-0.5}$ ($R^2 = 0.998$). Thus, a drug Fickian diffusion is again indicated in this timeframe, being present in the PLA hydrolysis (see Fig. 4B).

The Korsmeyer - Peppas and Peppas - Sahlin models were discarded for having inconsistent values of their parameters (see Fig. S8 (i) and (j), respectively, and Table TS2 in Supplementary Information).

Table 1 sums up in each frame of time the model providing the best fit together with its corresponding parameters value.

As an overview of the release mechanisms, it can be said that in the initial frame of time ($t \leq 48$ h) the release mechanism is dominated by two competing mechanisms, diffusion and relaxation of polymer chains, according to the Korsmeyer – Peppas model.

Similar release exponents are found in both 15 min and 40 min plasma treated samples, somewhat higher for the 40 min treated sample. This numerically result agrees with the qualitative observation of the slope in the experimental release curve (Fig. 4A) in the time range 0.5–48 h for these samples. In any case, its value indicates an anomalous transport mechanism following the Korsmeyer-Peppas model. Moreover, quite similar kinetics contants are found too, regardless of the treatment time.

In the second time range ($200h\rangle$ $t > 48$ h), the release process is based on the Fickian diffusion following the Higuchi's model, irrespective of the treatment. Again, kinetic constants are similar for both treated samples, but higher than that of the untreated one. It should be taken into account that the polylactic acid encapsulated in the hydrogel after plasma treatment was to some extent degraded in its oligomers and the hydrolysis process could take place more easily.

Although the drug diffusion coefficient is usually assumed to be independent of the drug concentration for computational simplicity, this dependence does exist, resulting in non-constant diffusion coefficients.

Several forms of the concentration-dependent diffusion coefficient were proposed in the bibliography (see, for instance, the review [42]) where concepts such as jumping of the solute through the medium, the free volume of the polymer matrix where molecules diffuse through free voids, the sieving impact of the polymeric chain structure on the diffusing molecules, or the crosslinking density in the matrix play a significant role in the diffusion process (Refs: [55]).

In our work, when the plasma treatment is applied, PLA is degraded in its oligomers and the subsequent degradation process by hydrolysis occurred more easily, giving rise to kinetic constants higher than that of the untreated sample. Nevertheless, no significant difference in this parameter is observed between the two treated samples (15 and 40 min).

Therefore, from the viewpoint of the kinetic constant, the plasma treatment time (for treated samples) seems no to play a noticeable role in both time frames. In order to propose a tentative explanation to this result two ideas should be combined.

On the one hand, the higher the plasma treatment time, the higher the available amount of lactic oligomers and the lactic acid itself (this was corroborated by FTIR and NMR results, see Sections 3.2.1 and 3.2.2). On the other hand, it should be also taken into account the impact on the release process of the physical interactions in which these oligomers participate, according to the rheological results and images obtained by SEM.

The schematic in Fig. 6 shows the interactions between the molecules of the ELR matrix and the PLA and its oligomers, that are present after the plasma treatment. Free amino groups from the lysine amino acids are

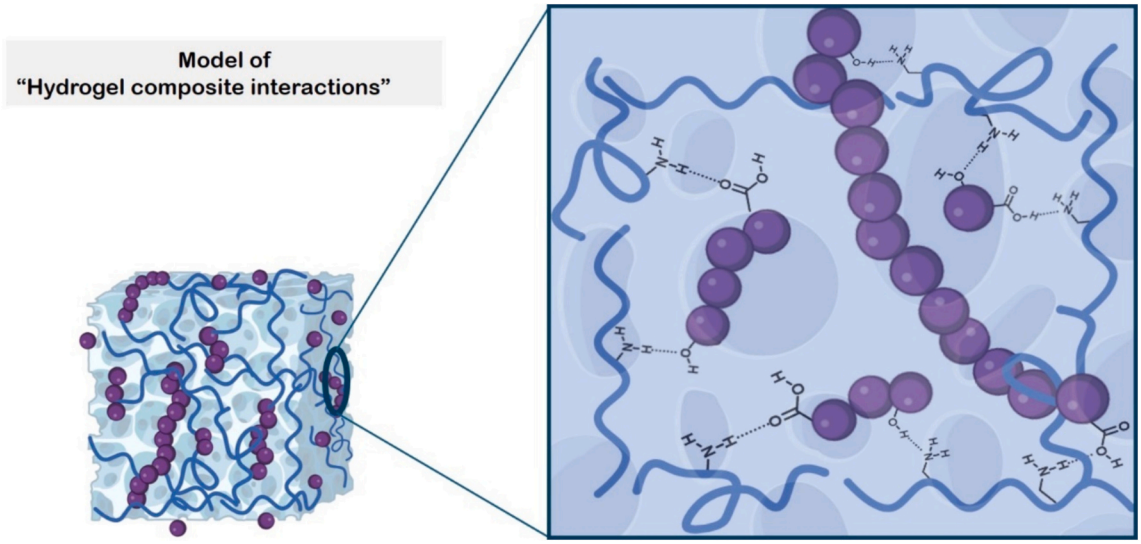

Fig. 6. Schematic at molecular level showing the physical interactions (hydrogen bonds) between the molecules of the ELR matrix and the PLA and its oligomers, that are present after the plasma treatment. Molecular chains in the ELR matrix are represented as continuous lines in blue colour, whereas lactic acid and oligomers are balls coloured in pink.

available in the ELRs polymeric network. The intermolecular interactions -e.g., by hydrogen bonds with the hydroxyl and carboxyl groups present in the generated oligomers- are shown in the zoom, in order to highlight the presence of physical crosslinking in the devices. The longer plasma treatment times, the higher proportion of oligomers (NMR data, Section 3.2.2), and this physical crosslinking contributes to a higher crosslinking density as it suggests the complex modulus magnitude increase with the time treatment (rheology measurements, Section 3.3.2).

It has been reported that the drug diffusion coefficient decreases as the physical crosslinking density increases, due to increased microstructural tortuosity and decreased space between macromolecular chains [56,57]. Thus, a trade-off is suggested between the greater hindrance to release exerted by the matrix due to the physical crosslinking in which the oligomers participate, and, at the same time, the greater accumulated amount of lactic acid, which would play an important regulatory role in the overall dynamic process of drug release. Consequently, the kinetic constants observed for the release in both treatments are very similar. This corroborates the results observed for the experimentally measured release and is also in agreement with the characterization of the properties studied.

According to these results, the release device designed as a composite has a threefold objective: first, an early release of lactic acid through the hydrogels is available, thus bringing forward its effect on cell behaviour; second, the modulation of this cumulative mass released at the beginning is achieved using the plasma treatment time as the control parameter; and third, a sustained release over time (for times longer than 150–200 h) due to PLA hydrolysis in aqueous media is observed.

5. Conclusions

The aim of this work has been to advance the research of new biomedical devices for application in cardiac tissue regeneration. The need for a biomaterial capable of releasing lactic acid (LA) in a controlled manner to sustain cardiomyocyte dedifferentiation, as an alternative to complex genetic reprogramming strategies, has been met. In this study, we have designed and implemented a biomedical device based on a nanocomposite hydrogel made from elastin-like recombinamer (ELR) polymers, which functions as an early, sustained, and regulated lactic acid release system. The novel developed nanocomposite hydrogel device can rapidly release lactic acid (LA) due to the initial partial degradation of PLA caused by the prior plasma treatment. This will promote a metabolic shift in the resident cardiomyocytes, enhancing their proliferative capacity from the start of the treatment and within a few hours after the cardiac injury, preventing scar tissue formation and presumably inducing an improvement in the functionality of the generated tissue. Moreover, it is capable of releasing LA in a sustained manner over time thanks to the hydrolysis of the encapsulated PLA. The selected treatment time is used as a control parameter to regulate the initial dose of LA released, observing a linear release profile of PLA over longer periods of more than 200 h (360 ng/h).

The extrusion tests and the injectability video using a 20G needle performed with the composite show appropriate shear-thinning behaviour and good injectability. Moreover, its rapid gelation will allow precise placement of the implant at the injury site without any diffusion. Likewise, the cell viability found for the PLA-treated composite, comparable to that of the standard control culture and the unloaded hydrogel itself, supports the potential application of the device in future trials to show its efficiency and possible application in the regeneration of infarcted tissue.

For all these reasons, it is worth noting that the designed implant allows for the immediate, controlled, and sustained release of lactate, which can be directly injected at the application site and has demonstrated good cytocompatibility. Future studies will assess both the efficacy of the system and the optimal timing for the application of this injectable device. In any case, this work lays the foundation for future research on cardiac tissue regeneration.

CRediT authorship contribution statement

Julio Fernández-Fernández: Writing – original draft, Methodology, Investigation. **Luis Quintanilla-Sierra:** Writing – review & editing, Writing – original draft, Validation, Supervision, Formal analysis. **Oscar Castaño:** Writing – review & editing, Validation, Funding acquisition. **Tosca Roncada:** Methodology, Investigation. **J. Carlos Rodríguez-Cabello:** Writing – review & editing, Validation, Resources, Funding acquisition. **Matilde Alonso:** Writing – review & editing, Validation, Supervision, Funding acquisition, Conceptualization. **Elisabeth Engel:** Writing – review & editing, Validation, Funding acquisition. **Mercedes Santos:** Writing – review & editing, Writing – original draft, Validation, Supervision, Funding acquisition, Conceptualization.

Declaration of competing interest

The authors declare that they have no known competing financial interests or personal relationships that could have appeared to influence the work reported in this paper.

Acknowledgement

The authors are grateful for funding from the Spanish Government (RTI2018-096320-B-C21, PID2021-122444OB-100, PID2022-137484OB-I00), the European Commission-Euronanomed nAngioderm Project (ref. JTC2018-103), the Pathfinder-EU project BIOACTION GA-101098972, Junta de Castilla y León (VA188P23), Junta de Castilla y León and FEDER Funds (CLU-2023-1-05), and Centro en Red de Medicina Regenerativa y Terapia Celular de Castilla y León.

Appendix A. Supplementary data

Supplementary data to this article can be found online at https://doi.org/10.1016/j.ijbiomac.2025.146552.

Data availability

No data was used for the research described in the article.

References

[1] Y. Zhang, C. Lin, M. Liu, W. Zhang, X. Xun, J. Wu, X. Li, Z. Luo, Burden and trend of cardiovascular diseases among people under 20 years in China, Western Pacific region, and the world: an analysis of the global burden of disease study in 2019, Front. Cardiovasc. Med. 10 (2023) 1067072, https://doi.org/10.3389/fcvm.2023.1067072.

[2] S.S. Virani, A. Alonso, H.J. Aparicio, E.J. Benjamin, M.S. Bittencourt, C. W. Callaway, A.P. Carson, A.M. Chamberlain, S. Cheng, F.N. Delling, M.S.V. Elkind, K.R. Evenson, J.F. Ferguson, D.K. Gupta, S.S. Khan, B.M. Kissela, K.L. Knutson, C. D. Lee, T.T. Lewis, J. Liu, M.S. Loop, P.L. Lutsey, J. Ma, J. Mackey, S.S. Martin, D. B. Matchar, M.E. Mussolino, S.D. Navaneethan, A.M. Perak, G.A. Roth, Z. Samad, G.M. Satou, E.B. Schroeder, S.H. Shah, C.M. Shay, A. Stokes, L.B. VanWagner, N.-Y. Wang, C.W. Tsao, Heart disease and stroke Statistics-2021 update: a report from the American Heart Association, Circulation 143 (2021) e254–e743, https://doi.org/10.1161/CIR.0000000000000950.

[3] M.A. Laflamme, C.E. Murry, Heart regeneration, Nature 473 (2011) 326–335, https://doi.org/10.1038/nature10147.

[4] L.I. Burd, M.D.J. Jones, M.A. Simmons, E.L. Makowski, G. Meschia, F.C. Battaglia, Placental production and foetal utilisation of lactate and pyruvate, Nature 254 (1975) 710–711, https://doi.org/10.1038/254710a0.

[5] J. Ordoño, S. Pérez-Amodio, K. Ball, A. Aguirre, E. Engel, The generation of a lactate-rich environment stimulates cell cycle progression and modulates gene expression on neonatal and hiPSC-derived cardiomyocytes, Biomater. Adv. 139 (2022) 213035, https://doi.org/10.1016/j.bioadv.2022.213035.

[6] L. Sun, J. Yu, S. Qi, Y. Hao, Y. Liu, Z. Li, Bone morphogenetic protein-10 induces cardiomyocyte proliferation and improves cardiac function after myocardial infarction, J. Cell. Biochem. 115 (2014) 1868–1876, https://doi.org/10.1002/jcb.24856.

[7] H. Chen, W. Yong, S. Ren, W. Shen, Y. He, K.A. Cox, W. Zhu, W. Li, M. Soonpaa, R. M. Payne, D. Franco, L.J. Field, V. Rosen, Y. Wang, W. Shou, Overexpression of bone morphogenetic protein 10 in myocardium disrupts cardiac postnatal hypertrophic growth, J. Biol. Chem. 281 (2006) 27481–27491, https://doi.org/10.1074/jbc.M604818200.

[8] W.J. Richardson, S.A. Clarke, T.A. Quinn, J.W. Holmes, Physiological implications of myocardial scar structure, Compr. Physiol. 5 (2015) 1877–1909, https://doi.org/10.1002/cphy.c140067.

[9] P. Blasi, Poly(lactic acid)/poly(lactic-co-glycolic acid)-based microparticles: an overview, J. Pharm. Investig. 49 (2019) 337–346, https://doi.org/10.1007/s40005-019-00453-z.

[10] A.K. Gaharwar, N.A. Peppas, A. Khademhosseini, Nanocomposite hydrogels for biomedical applications, Biotechnol. Bioeng. 111 (2014) 441–453, https://doi.org/10.1002/bit.25160.

[11] F. Karchoubi, R. Afshar Ghotli, H. Pahlevani, M. Baghban Salehi, New insights into nanocomposite hydrogels; a review on recent advances in characteristics and applications, Adv. Ind. Eng. Polym. Res. 7 (2024) 54–78, https://doi.org/10.1016/j.aiepr.2023.06.002.

[12] P. Thoniyot, M.J. Tan, A.A. Karim, D.J. Young, X.J. Loh, Nanoparticle–hydrogel composites: concept, design, and applications of these promising, multi-functional materials, Adv. Sci. 2 (2015) 1400010, https://doi.org/10.1002/advs.201400010.

[13] M.M. El Sayed, Production of polymer hydrogel composites and their applications, J. Polym. Environ. 31 (2023) 2855–2879, https://doi.org/10.1007/s10924-023-02796-z.

[14] N.L. Hancox, Engineering Mechanics of Composite Materials, 1996, https://doi.org/10.1016/s0261-3069(97)87195-6.

[15] S. Rafieian, H. Mirzadeh, H. Mahdavi, M.E. Masoumi, A Review on Nanocomposite Hydrogels and Their Biomedical Applications 26, 2019, pp. 154–174, https://doi.org/10.1515/secm-2017-0161.

[16] P. Zhang, J. Qi, R. Zhang, Y. Zhao, J. Yan, Y. Gong, X. Liu, B. Zhang, X. Wu, X. Wu, C. Zhang, B. Zhao, B. Li, Recent advances in composite hydrogels: synthesis, classification, and application in the treatment of bone defects, Biomater. Sci. 12 (2024) 308–329, https://doi.org/10.1039/D3BM01795H.

[17] X. Liao, X. Yang, H. Deng, Y. Hao, L. Mao, R. Zhang, W. Liao, M. Yuan, Injectable hydrogel-based nanocomposites for cardiovascular diseases, Front. Bioeng. Biotechnol. 8 (2020) 251, https://doi.org/10.3389/fbioe.2020.00251.

[18] S.A. Maskarinec, D.A. Tirrell, Protein engineering approaches to biomaterials design, Curr. Opin. Biotechnol. 16 (2005) 422–426, https://doi.org/10.1016/j.copbio.2005.06.009.

[19] S. Roberts, M. Dzuricky, A. Chilkoti, Elastin-like polypeptides as models of intrinsically disordered proteins, FEBS Lett. 589 (2015) 2477–2486, https://doi.org/10.1016/j.febslet.2015.08.029.

[20] F.J. Arias, M. Santos, A. Fernández-Colino, G. Pinedo, A. Girotti, Recent contributions of elastin-like recombinamers to biomedicine and nanotechnology, Curr. Top. Med. Chem. 14 (2014) 819–836, https://doi.org/10.2174/1568026614666140118223412.

[21] J.C. Rodríguez-Cabello, F.J. Arias, M.A. Rodrigo, A. Girotti, Elastin-like polypeptides in drug delivery, Adv. Drug Deliv. Rev. 97 (2016) 85–100, https://doi.org/10.1016/j.addr.2015.12.007.

[22] M.H. Misbah, L. Quintanilla-Sierra, M. Alonso, J.C. Rodríguez-Cabello, M. Santos, "In-situ" formation of elastin-like recombinamer hydrogels with tunable viscoelasticity through efficient one-pot process, Mater. Today Bio. 25 (2024) 100999, https://doi.org/10.1016/j.mtbio.2024.100999.

[23] D. Zhu, H. Wang, P. Trinh, S.C. Heilshorn, F. Yang, Elastin-like protein-hyaluronic acid (ELP-HA) hydrogels with decoupled mechanical and biochemical cues for cartilage regeneration, Biomaterials 127 (2017) 132–140, https://doi.org/10.1016/j.biomaterials.2017.02.010.

[24] J.C. Rodríguez-Cabello, I. González de Torre, A. Ibañez-Fonseca, M. Alonso, Bioactive scaffolds based on elastin-like materials for wound healing, Adv. Drug Deliv. Rev. 129 (2018) 118–133, https://doi.org/10.1016/j.addr.2018.03.003.

[25] E. Tejeda-Montes, A. Klymov, M.R. Nejadnik, M. Alonso, J.C. Rodriguez-Cabello, X. F. Walboomers, A. Mata, Mineralization and bone regeneration using a bioactive elastin-like recombinamer membrane, Biomaterials 35 (2014) 8339–8347, https://doi.org/10.1016/j.biomaterials.2014.05.095.

[26] A. Fernández-Colino, F. Wolf, S. Rütten, T. Schmitz-Rode, J.C. Rodríguez-Cabello, S. Jockenhoevel, P. Mela, Small caliber compliant vascular grafts based on elastin-like recombinamers for in situ tissue engineering, Front. Bioeng. Biotechnol. 7 (2019), https://doi.org/10.3389/fbioe.2019.00340.

[27] A. Ibáñez-Fonseca, S. Santiago Maniega, D. Gorbenko Del Blanco, B. Catalán Bernardos, A. Vega Castrillo, Á.J. Álvarez Barcia, M. Alonso, H.J. Aguado, J. C. Rodríguez-Cabello, Elastin-like recombinamer hydrogels for improved skeletal muscle healing through modulation of macrophage polarization, Front. Bioeng. Biotechnol. 8 (2020) 413, https://doi.org/10.3389/fbioe.2020.00413.

[28] T. Flora, I. González de Torre, M. Alonso, J.C. Rodríguez-Cabello, Use of proteolytic sequences with different cleavage kinetics as a way to generate hydrogels with preprogrammed cell-infiltration patterns imparted over their given 3D spatial structure, Biofabrication 11 (2019) 35008, https://doi.org/10.1088/1758-5090/ab10a5.

[29] F. González-Pérez, A. Ibáñez-Fonseca, M. Alonso, J.C. Rodríguez-Cabello, Combining tunable proteolytic sequences and a VEGF-mimetic peptide for the spatiotemporal control of angiogenesis within elastin-like recombinamer scaffolds, Acta Biomater. 130 (2021) 149–160, https://doi.org/10.1016/j.actbio.2021.06.005.

[30] F. González-Pérez, S. Acosta, S. Rütten, C. Emonts, A. Kopp, H.-W. Henke, P. Bruners, T. Gries, J.C. Rodríguez-Cabello, S. Jockenhoevel, A. Fernández-Colino, Biohybrid elastin-like venous valve with potential for in situ tissue engineering, Front. Bioeng. Biotechnol. 10 (2022), https://doi.org/10.3389/fbioe.2022.988533.

[31] I. González De Torre, M. Santos, L. Quintanilla, A. Testera, M. Alonso, J. C. Rodríguez Cabello, Elastin-like recombinamer catalyst-free click gels: characterization of poroelastic and intrinsic viscoelastic properties, Acta Biomater. 10 (2014) 2495–2505, https://doi.org/10.1016/j.actbio.2014.02.006.

[32] H.C. Kolb, M.G. Finn, K.B. Sharpless, Click chemistry: diverse chemical function from a few good reactions, Angew. Chem. Int. Ed. Eng. 40 (2001) 2004–2021, https://doi.org/10.1002/1521-3773(20010601)40:11<2004::AID-ANIE2004>3.0.CO;2-5.

[33] M. González-Pérez, D.B. Camasão, D. Mantovani, M. Alonso, J.C. Rodríguez-Cabello, Biocasting of an elastin-like recombinamer and collagen bi-layered model of the tunica adventitia and external elastic lamina of the vascular wall, Biomater. Sci. 9 (2021) 3860–3874, https://doi.org/10.1039/D0BM02197K.

[34] F. Chen, P. Le, G.M. Fernandes-Cunha, S.C. Heilshorn, D. Myung, Bio-orthogonally crosslinked hyaluronate-collagen hydrogel for suture-free corneal defect repair, Biomaterials 255 (2020) 120176, https://doi.org/10.1016/j.biomaterials.2020.120176.

[35] J.C. Rodríguez-Cabello, L. Martín, M. Alonso, F.J. Arias, A.M. Testera, "Recombinamers" as advanced materials for the post-oil age, Polymer (Guildf.) 50 (2009) 5159–5169, https://doi.org/10.1016/j.polymer.2009.08.032.

[36] A. Girotti, D. Orbanic, A. Ibáñez-Fonseca, C. Gonzalez-Obeso, J.C. Rodríguez-Cabello, Recombinant technology in the development of materials and systems for

soft-tissue repair, Adv. Healthc. Mater. 4 (2015) 2423–2455, https://doi.org/10.1002/adhm.201500152.
[37] T. Flora, I.G. de Torre, M. Alonso, J.C. Rodríguez-Cabello, Tethering QK peptide to enhance angiogenesis in elastin-like recombinamer (ELR) hydrogels, J. Mater. Sci. Mater. Med. 30 (2019) 30, https://doi.org/10.1007/s10856-019-6232-z.
[38] A. Ibáñez-Fonseca, T. Flora, S. Acosta, J.C. Rodríguez-Cabello, Trends in the design and use of elastin-like recombinamers as biomaterials, Matrix Biol. 84 (2019) 111–126, https://doi.org/10.1016/j.matbio.2019.07.003.
[39] L. Quintanilla-Sierra, C. García-Arévalo, J.C. Rodriguez-Cabello, Self-assembly in elastin-like recombinamers: a mechanism to mimic natural complexity, Mater. Today Bio. 2 (2019), https://doi.org/10.1016/j.mtbio.2019.100007.
[40] P. Contessotto, D. Orbanić, M. Da Costa, C. Jin, P. Owens, S. Chantepie, C. Chinello, J. Newell, F. Magni, D. Papy-Garcia, N.G. Karlsson, M. Kilcoyne, P. Dockery, J. C. Rodríguez-Cabello, A. Pandit, Elastin-like recombinamers-based hydrogel modulates post-ischemic remodeling in a non-transmural myocardial infarction in sheep, Sci. Transl. Med. 13 (2021) eaaz5380, https://doi.org/10.1126/scitranslmed.aaz5380.
[41] W.I. Higuchi, Diffusional models useful in biopharmaceutics. Drug release rate processes, J. Pharm. Sci. 56 (1967) 315–324, https://doi.org/10.1002/jps.2600560302.
[42] J. Siepmann, N.A. Peppas, Higuchi equation: derivation, applications, use and misuse, Int. J. Pharm. 418 (2011) 6–12, https://doi.org/10.1016/j.ijpharm.2011.03.051.
[43] N.A. Peppas, J.J. Sahlin, A simple equation for the description of solute release. III. Coupling of diffusion and relaxation, Int. J. Pharm. 57 (1989) 169–172, https://doi.org/10.1016/0378-5173(89)90306-2.
[44] R.W. Korsmeyer, R. Gurny, E. Doelker, P. Buri, N.A. Peppas, Mechanisms of solute release from porous hydrophilic polymers, Int. J. Pharm. 15 (1983) 25–35, https://doi.org/10.1016/0378-5173(83)90064-9.
[45] P. Arany, E. Róka, L. Mollet, A.W. Coleman, F. Perret, B. Kim, R. Kovács, A. Kazsoki, R. Zelkó, R. Gesztelyi, Z. Ujhelyi, P. Fehér, J. Váradi, F. Fenyvesi, M. Vecsernyés, I. Bácskay, Fused deposition modeling 3D printing: test platforms for evaluating post-fabrication chemical modifications and in-vitro biological properties, Pharmaceutics 11 (2019), https://doi.org/10.3390/pharmaceutics11060277.
[46] Y. Peng, W. Wang, J. Cao, Preparation of sodium ligninsulfonate-layered double hydroxide and its effects on wood flour/polypropylene composites during accelerated UV weathering, Polym. Compos. 39 (2018) 2451–2460, https://doi.org/10.1002/pc.24230.
[47] E. Fumoto, S. Sato, Y. Kawamata, Y. Koyama, T. Yoshikawa, Y. Nakasaka, T. Tago, T. Masuda, Determination of carbonyl functional groups in lignin-derived fraction using infrared spectroscopy, Fuel 318 (2022) 123530, https://doi.org/10.1016/j.fuel.2022.123530.
[48] K.V. Holmberg, M. Abdolhosseini, Y. Li, X. Chen, S.-U. Gorr, C. Aparicio, Bio-inspired stable antimicrobial peptide coatings for dental applications, Acta Biomater. 9 (2013) 8224–8231, https://doi.org/10.1016/j.actbio.2013.06.017.
[49] J.L. Espartero, I. Rashkov, S.M. Li, N. Manolova, M. Vert, NMR analysis of low molecular weight poly(lactic acid)s, Macromolecules 29 (1996) 3535–3539, https://doi.org/10.1021/ma950529u.
[50] A. Vedadghavami, F. Minooei, M.H. Mohammadi, S. Khetani, A. Rezaei Kolahchi, S. Mashayekhan, A. Sanati-Nezhad, Manufacturing of hydrogel biomaterials with controlled mechanical properties for tissue engineering applications, Acta Biomater. 62 (2017) 42–63, https://doi.org/10.1016/j.actbio.2017.07.028.
[51] Q. Liu, X. Dong, H. Qi, H. Zhang, T. Li, Y. Zhao, G. Li, W. Zhai, 3D printable strong and tough composite organo-hydrogels inspired by natural hierarchical composite design principles, Nat. Commun. 15 (2024) 3237, https://doi.org/10.1038/s41467-024-47597-7.
[52] F. Tantakitti, J. Boekhoven, X. Wang, R.V. Kazantsev, T. Yu, J. Li, E. Zhuang, R. Zandi, J.H. Ortony, C.J. Newcomb, L.C. Palmer, G.S. Shekhawat, M.O. de la Cruz, G.C. Schatz, S.I. Stupp, Energy landscapes and functions of supramolecular systems, Nat. Mater. 15 (2016) 469–476, https://doi.org/10.1038/nmat4538.
[53] F. Cipriani, M. Krüger, I.G. de Torre, L.Q. Sierra, M.A. Rodrigo, L. Kock, J. C. Rodriguez-Cabello, Cartilage regeneration in preannealed silk elastin-like co-recombinamers injectable hydrogel embedded with mature chondrocytes in an ex vivo culture platform, Biomacromolecules 19 (2018) 4333–4347, https://doi.org/10.1021/acs.biomac.8b01211.
[54] M. Dusselier, P. Van Wouwe, A. Dewaele, E. Makshina, B.F. Sels, Lactic acid as a platform chemical in the biobased economy: the role of chemocatalysis, Energy Environ. Sci. 6 (2013) 1415–1442, https://doi.org/10.1039/C3EE00069A.
[55] C.-C. Lin, A.T. Metters, Hydrogels in controlled release formulations: network design and mathematical modeling, Adv. Drug Deliv. Rev. 58 (2006) 1379–1408, https://doi.org/10.1016/j.addr.2006.09.004.
[56] T. Canal, N.A. Peppas, Correlation between mesh size and equilibrium degree of swelling of polymeric networks, J. Biomed. Mater. Res. 23 (1989) 1183–1193, https://doi.org/10.1002/jbm.820231007.
[57] N.A. Peppas, P. Bures, W. Leobandung, H. Ichikawa, Hydrogels in pharmaceutical formulations, Eur. J. Pharm. Biopharm. Off. J. Arbeitsgemeinschaft Fur Pharm. Verfahrenstechnik e.V. 50 (2000) 27–46, https://doi.org/10.1016/s0939-6411(00)00090-4.